RECENT RESULTS FROM THE H1 COLLABORATION AT HERA[1]

J. FELTESSE
CEA, DAPNIA/DSM/ Service de Physique des Particules, CE-Saclay
F-91191 *Gif-sur-Yvette Cedex, France*

Abstract

New results from the H1 experiment at the electron-proton collider HERA are reported.

As a complement to the results on photoproduction which are detailed in an other report in these proceedings, evidence for hard scattering in gamma diffraction in photoproduction events is presented.

The hadronic final state in low x deep inelastic scattering (DIS) events has been analysed. Transverse energy flow and cross section for production of jets at high x_j are compared to the expectations of present Monte Carlo programs and to analytical calculations based on the BFKL evolution equation.

DIS interactions with no hadronic energy flow in a large interval of rapidity around the incident proton direction are presented. The data are compared to models based on deep inelastic pomeron scattering or on VMD contributions.

Measured cross sections for the production of multijet in DIS events at HERA are used to provide a preliminary measurement of the strong coupling constant α_s together with the first direct measurement of the gluon density in the proton.

The cross section of the charged current process $e^- p \rightarrow \nu_e + hadrons$ is measured. The effects of the W propagator term is visible for the first time.

New limits on leptoquarks, leptogluons, Squarks from R-parity violating supersymmetry and on excited leptons are given.

1. Introduction

On May 31st 1992, the H1 collaboration recorded the first identified deep inelastic event produced at the new collider HERA in which 26.7 GeV energy electrons collide with 820 GeV protons. The squared momentum transfer of the interaction was $Q^2 = 18$ GeV^2, a value in the range of previous lepton-nucleon scattering experiments on fixed targets. But in this event x, the fraction of the proton momentum carried by the struck quark, also called Bjorken x, was $x = 0.0004$, a value hundred times smaller than had ever before been achieved at this Q^2 value. Eight years after the approval of HERA a new domain of physics was opened by the HERA experiments H1 [1] and ZEUS [2]. Since may 1992, the luminosity has gradually increased. In

[1] Invited talk at the Deep Inelastic Scattering workshop in Eilat, February 13-25, 1994.

1992 the integrated luminosity recorded by the H1 experiment was about $25 nb^{-1}$ and jumped to 530 nb^{-1} in 1993. The length of the interaction region has also decreased by almost a factor 2 between 1992 and 1993 thus allowing better conditions to reduce the background (see Fig.1).

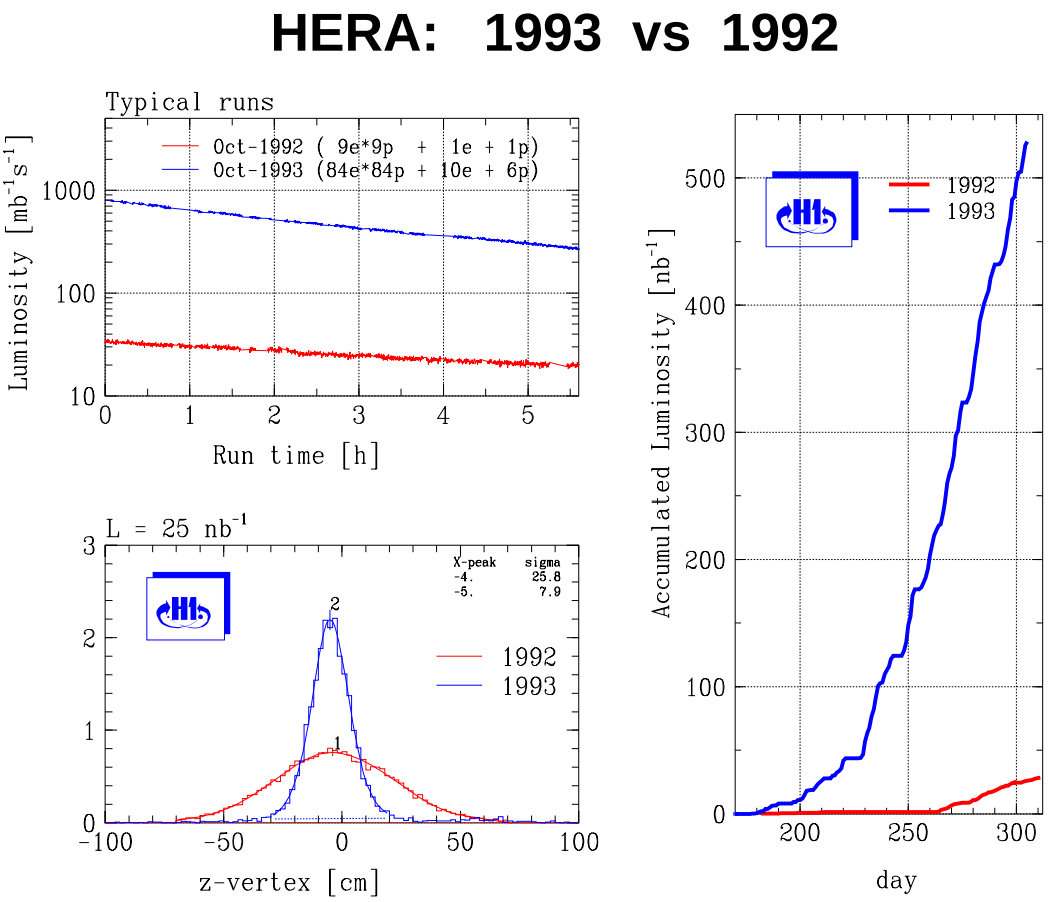

Figure 1: Luminosity and distribution of the interaction point in 1992 and 1993.

The maximum peak luminosity per second has reached $1.5\,10^{30}\,cm^{-2}\,s^{-1}$ which is 10% of the design value. Unfortunately, due to a Helium leak in the main solenoid of the H1 detector , about 20% of the data were taken without magnetic field.

Three months after the end of the data taking period, only part of the available statistics have been used in most of the analyses. The runs where some part of the detector was not working properly have been left for further investigations, especially those with no field.

In this talk, after a short description of the H1 detector, I present recent results on the many physics processes which can be studied at HERA, ranked by decreasing cross sections :

-Photoproduction of almost real photons. Cross section : 20 μb.
-Neutral Current Deep Inelastic Scattering. Cross section at $Q^2 > 5$ GeV^2 : 100 nb.
-Charged Current Deep Inelastic Scattering. Cross section : 100 pb.
-Searches beyond the Standard Model. Cross section limits : 10 pb.

2. The H1 Detector

In the following a coordinate system with origin at the interaction point and z axis along the proton, or forward, direction is used. Polar angles θ are measured relative to the proton direction. The pseudo-rapidity of a final state particle with polar angle θ is $\eta = -\ln\tan\frac{\theta}{2}$.

The H1 detector [1] is a large multi-purpose detector of a size comparable to those at LEP (see Fig.2). The tracking systems and the calorimeters are more extended in the forward direction due to the asymmetry of the proton and electron beam energies.

The backbone of the H1 detector is the finely segmented liquid argon calorimeter. It is divided into electromagnetic and hadronic sections, with lead and steel absorber respectively. The liquid argon provides a very stable response (better than 0.5 % per year). The pseudo-rapidity which may be measured in the liquid argon calorimeter ranges from -1.5 to 3.65. The calorimeter coverage is completed with a small calorimeter with copper absorber and silicon pad readout in the very forward direction ($\theta < 4^0$) and a conventional electromagnetic lead-scintillator sandwich calorimeter (BEMC) in the backward direction ($\theta > 151^0$). The backward region corresponds to small electron angle scattering, that is the low Q^2 region.

The central tracking detector consists of a hybrid of inner and outer jet chambers, z drift chambers and proportional chambers. The forward tracking detector is an array of drift and proportional chambers which extend track measurement into the forward direction.

The calorimeter and the tracking system are placed inside a superconducting solenoid which, together with the surrounding octagonal iron flux return yoke, maintains a uniform magnetic field of 1.2 T along z in the tracking volume. The iron yoke is instrumented with streamer tubes for muon measurement. Additional analogue read-out facilitates detection of hadronic energy escaping from rear of the liquid argon hadronic calorimeter.

The forward muon system enhances muon identification and measurement in the forward direction.

The luminosity is determined by measuring the Compton process $ep \to ep\,\gamma$ at very small scattering angle. The electron and the photon are detected in counters (labelled ET and PD in fig.2) situated at 33 m and 103 m respectively from the interaction point. The electron detector allows tagging of electrons scattered at small angles ($< 5\,mrad$) in photoproduction processes.

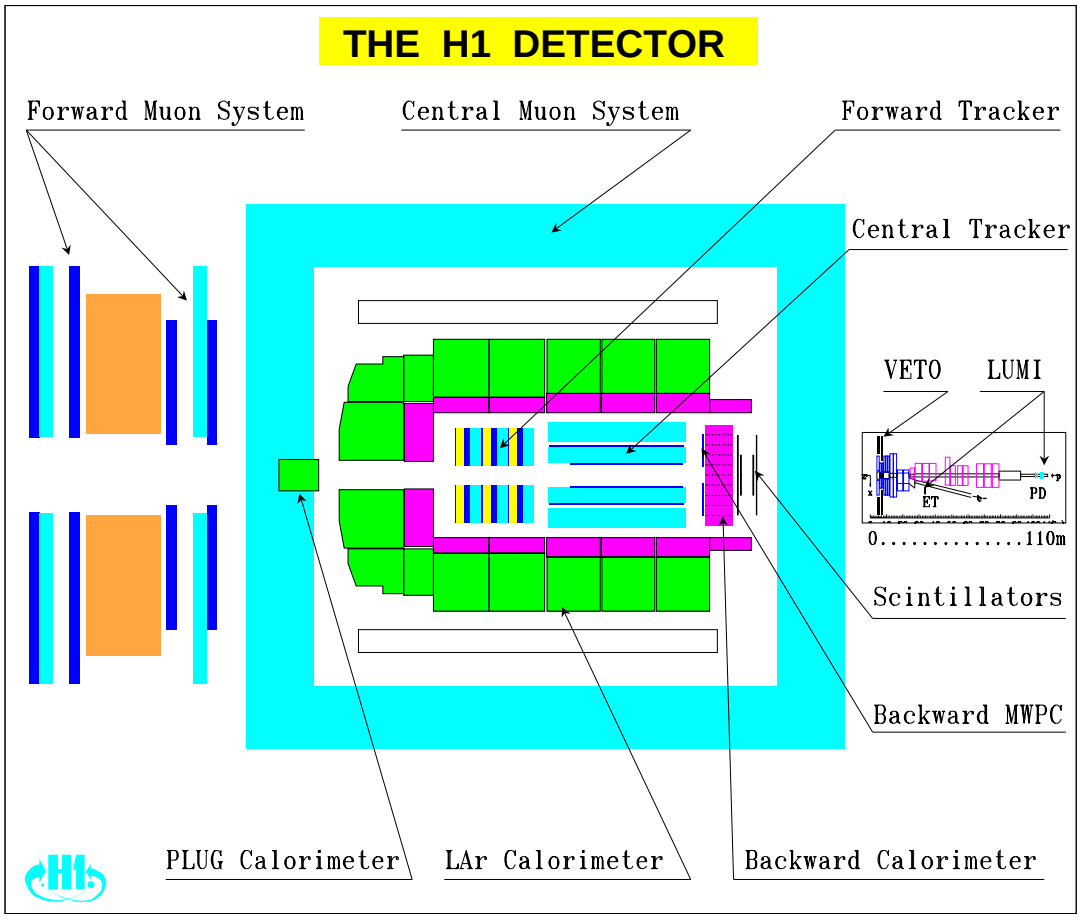

Figure 2: Schematic transversal view of the H1 detector. Note that the luminosity detector, downstream in the electron beam is not to scale.

3. Physics of almost real photons

In most of the interactions at HERA the electron interacts with the proton through the exchange of a virtual photon. When the scattered electron is emitted at very low angle and detected in the electron tagger (ET) the negative mass squared of the virtual photon, Q^2, is close to zero (10^{-7} GeV$^2 < Q^2 < 10^{-2}$ GeV^2), the virtual photon is almost real. Thus it is possible to study collisions of almost real photons with electrons and protons at centre of mass energies of about 200 GeV.

From the analysis of the data recorded in 1992 we have determined the following very important properties of the interaction of photons with nucleons at very high energy :

-Like in hadron hadron interactions, the total cross section rises weakly from the fixed target domain to HERA energies.

-The large tail of the transverse momentum distribution of charged particles shows however that when interacting with a proton the photon behaves differently

than a hadron at the same centre of mass energy.

-At large transverse momentum the photon interacts either directly with a quark or a gluon in the proton (direct processes) or indirectly when a parton issued from the photon interacts with a parton of the proton (resolved processes).

-The study of resolved processes shows a large sensitivity to the gluon content of the photon.

With the data recorded in 1993 it is possible to do more quantitative analyses. We are at present close to being able to extract the gluon density of the photon. All these aspects of the interactions of almost real photons with protons are developed in detail in an other report of these proceedings [3] and will not be repeated here. Let me just add a few words on a complementary aspect of photoproduction at HERA : the observation of hard scattering in diffractive processes.

As for hadrons it is expected that a large fraction of the interactions of almost real photons with nucleons is due to the photon diffractive dissociation. In the H1 detector diffractive events can be characterised by a small value of η_{max} which is defined, for each event, as the largest forward pseudo-rapidity of all liquid argon calorimeter clusters. A cluster is an isolated set of adjacent cells with a summed energy of at least 0.4 GeV. The distribution of η_{max} for tagged photoproduction events is shown in Fig.3. In most of the events there is energy close to the largest pseudo-rapidity which can be detected in the liquid argon detector. There is also a class of events in which η_{max} is small or even negative. The data are compared with the results of a Monte Carlo simulation based on the PYTHIA generator [4]. The simulation includes non diffractive hard scattering processes (nd) and soft diffractive scattering processes (sd) of the photon on the proton based on the final state phase space configuration. The soft diffractive model (sd) does not include hard scattering. The measured η_{max} distribution is well reproduced by the sum of these two contributions.

To investigate further the properties of the diffractive events we select the events with $\eta_{max} < 1$. Distribution of the transverse momentum of the charged tracks of diffractive events (Fig.4) shows a significant excess of charged particles at high transverse momentum which is not described by the 'soft' Monte Carlo (dashed line). The data are also compared with a model (POMPYT [5]) of hard diffractive scattering based on exchange of a pomeron between the proton and the virtual photon and in which the virtual photon interacts with a parton constituent of the pomeron. The high transverse momentum distribution of the data is well described by this model and can be then considered as a first indication of hard scattering in diffractive processes in photoproduction. Even stronger evidence comes from the η_{max} distribution of photoproduction events which contain at least one jet of transverse energy above 4 GeV (Fig.5). There is an excess of events at low rapidity ($\eta_{max} < 1.5$) over the expectation of the non diffractive hard scattering model (PYTHIA), which is well described by the hard diffractive scattering model POMPYT.

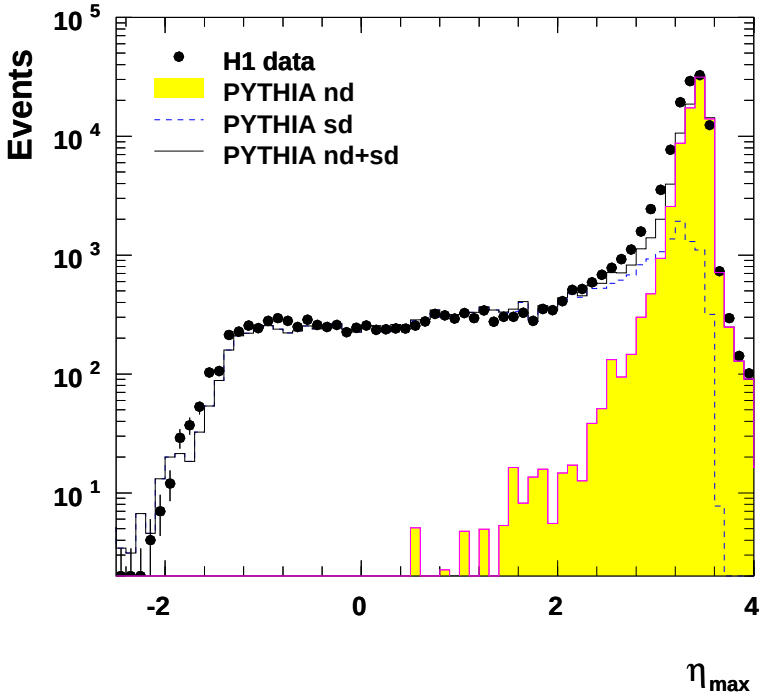

Figure 3: The η_{max} distribution of photoproduction data compared with PYTHIA non-diffractive (nd) and diffractive (sd) and the sum therof (nd+sd).

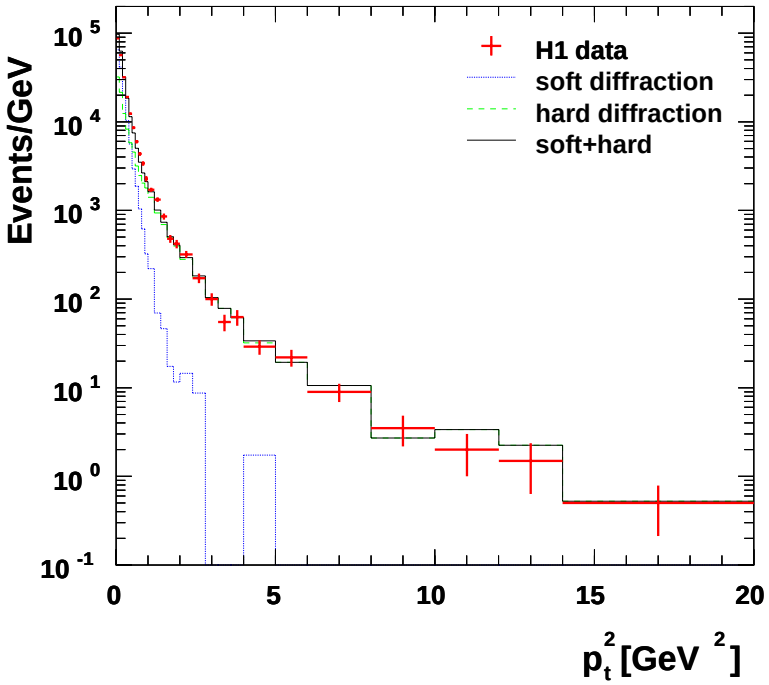

Figure 4: The p_t^2 distribution of rapidity gap photoproduction events compared with the PYTHIA soft diffraction expectation, the POMPYT hard diffraction and the sum thereof .

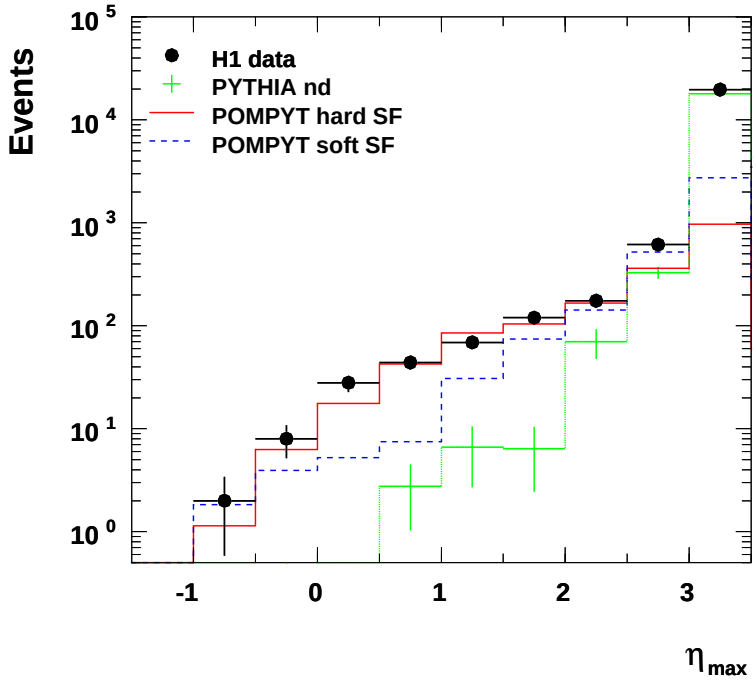

Figure 5: The η_{max} distribution of photoproduction events with at least one jet with a transverse energy $Ejet_T > 4$ GeV, compared with the PYTHIA non-diffractive and POMPYT expectations. A hard or a soft structure function of the pomperon has been used in the POMPYT simulations.

4. Deep Inelastic Scattering

When Q^2, the squared mass of the virtual photon, exceeds a few GeV^2, the scattering is deeply inelastic. At HERA a new regime in deep inelastic scattering is investigated. The highest Q^2 reached in the data is a few 10^4 GeV^2 at large x and the lowest x is 10^{-4} at $Q^2 \simeq 5$ GeV^2. Small x deep inelastic scattering probes QCD in a region where a novel QCD dynamics, based on the BFKL evolution equation [6], is expected. The main physics message of the data of 1992 is the first observation by the H1 and ZEUS collaborations of the rise of the structure function F_2 with decreasing x [7, 8]. Past experience on fixed target experiments have demonstrated how the measurement of structure functions is dramatically sensitive to unknown systematics effects. The H1 collaboaration has chosen not to show measurements of F_2 with the data of 1993 before the systematics are fully under control, but rather to concentrate at this workshop on the study of the very rich hadronic final state in deep inelastic scattering events.

4.1 Energy flow in DIS events

In the naive quark-parton model the transverse momentum of the scattered electron is balanced by a single jet associated with the struck quark, usually called the current jet. Higher-order QCD processes modify this picture. In the low x domain, the region away from the expected current jet towards the proton remnant is of particular interest in the analysis of the energy flow, as it may be the region most sensitive to new effects based on BFKL dynamics [6]. Expectations for the properties of hadronic final states are available in the form of Monte Carlo models, which are based on standard QCD evolution but differ widely in their predictions. The MEPS model is an option of the LEPTO generator [9] based on GLAP dynamics [10]. It combines rigorous LO matrix elements and an approximate treatment of higher order effects with leading-log parton showers. The PSWQ model is an other option of the LEPTO generator based on the parton shower model where the virtuality of the emitting gluon is set to WQ, where W is the invariant mass of the hadronic final state. The CDM model [11] provides an implementation of the colour dipole model of a chain of independent radiating dipoles connected via the emitting gluons. The HERWIG generator [12] provides a leading log parton shower model obeying coherence in both the initial and final state cascade.

Transverse energy flows, transverse energy-energy correlations and charged particle spectra have been studied [13]. The data presented here correspond to an integrated luminosity of 22.5 nb^{-1}. The transverse energy flow in the laboratory system corrected for detector effects is presented in Fig. 6 as a function of the pseudorapidity distance $\Delta\eta = \eta - \eta_q$. Here $\eta_q = -\ln\tan\frac{\theta_q}{2}$ is the current jet direction in the quark parton model (QPM) and can be calculated from the kinematic variables x and Q^2 of the scattered electron. The maximum E_T flow around the current jet direction is always shifted towards the direction of the proton remnant, the shift being larger

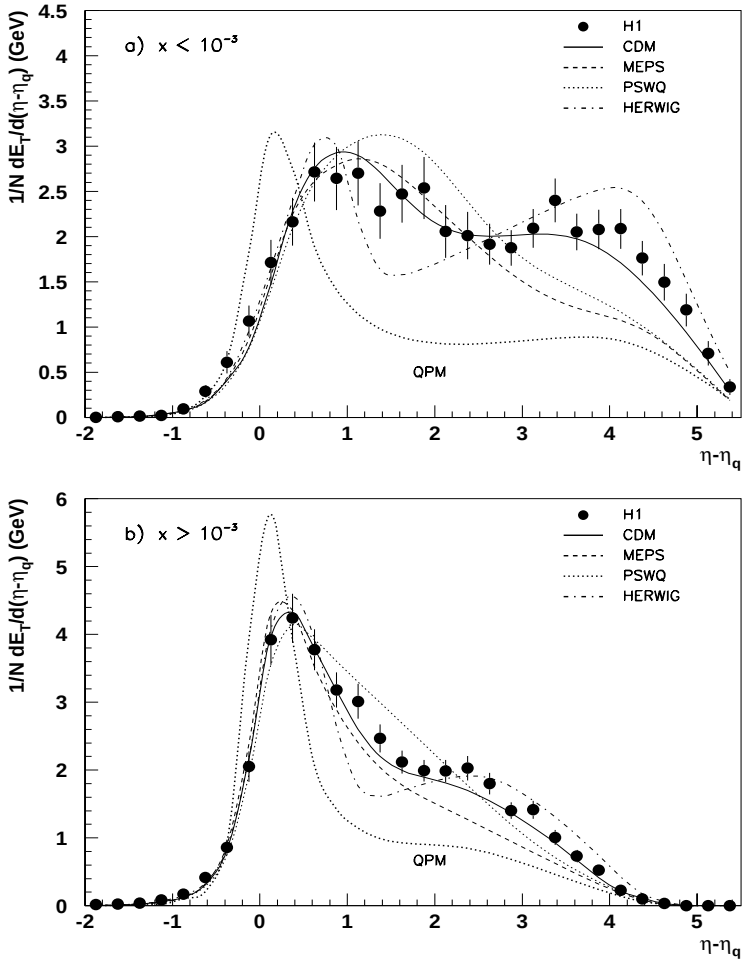

Figure 6: Transverse energy flows E_T in the laboratory system as a function of the pseudorapidity distance to the current jet quark' $\eta - \eta_q$ for events with **a)** $x < 10^{-3}$ and **b)** $x > 10^{-3}$. The proton direction is to the right. The error bars contain the statistical and systematic errors added in quadrature, except for an overall 6% energy scale uncertainty.

x range	Data	MEPS $MRSD0$	MEPS $MRSD^-$	CDM
$2\,10^{-4}$ *to* $2\,10^{-3}$	$128 \pm 12 \pm 26$	69	53	32
$2\,10^{-4}$ *to* $1\,10^{-3}$	$85 \pm 9 \pm 17$	37	27	21
$1\,10^{-4}$ *to* $2\,10^{-3}$	$43 \pm 7 \pm 9$	32	26	11

Table 1: Number of DIS events with a selected forward jet.

at small x. Comparing with the QPM curve, which is strongly peaked very close to the current quark direction, the shift observed in the data can be attributed to QCD radiation. For $x < 10^{-3}$ the data show a plateau of $E_T \approx 2$ GeV per unit of rapidity away from the current quark , the drop at $\Delta\eta \geq 4$ is due to the detector acceptance. For the large x data the maximum E_T is higher. A plateau is not observed, because the event kinematics boosts the hadronic system more into the forward region and the detector acceptance has a severe effect on the measurements for $\Delta\eta \geq 2.5$. The investigated QCD models offer a large variety of predictions for the presented energy flow measurements. Only the colour dipole model (CDM) is in reasonable agreement with the data. All other models differ significantly from the data with respect to the shape of the distributions and/or the absolute amount of transverse energy, in particular towards the remnant direction. The high value of E_T can be compared to analytic calculations [14] based on BFKL dynamics which predict a fairly flat plateau at low x with $E_T \approx 2$ GeV per unit of rapidity but much less E_T if GLAP dynamics is assumed. However this is not yet a conclusive evidence because no hadronization has been included in these calculations.

4.2 Forward jets in DIS events

An other possible footprint of the BFKL dynamics is the rate of jets produced in a deep inelastic event as sketched in Fig. 7. In order to be more sensitive to the BFKL dynamics, the transverse size $1/k_{jt}$ of the selected jet should be close to $1/Q$, the momentum fraction x_j of the jet should be as large as possible whereas the momentum fraction x of the quark struck by the virtual photon should be as small as possible. In a sample of DIS events with $Q^2 \approx 20$ GeV^2 and $2\,10^{-4} < x < 2\,10^{-3}$, we have counted the jets with $x_j > 0.05$ and $0.5 < k_{jt}^2/Q^2 < 6$. The resulting number of events is given in Table 1 and compared to expectations of the MEPS and CDM models simulated in our detector. We can see that the predictions tend to be below the observations and do not depend significantly on the parametrization of structure functions ($MRSD0$ [15] or $MRSD^-$ [16]). The size of the errors do not allow yet a firm conclusion. We can however notice that the rate of jets rises with decreasing x as expected from BFKL dynamics [17].

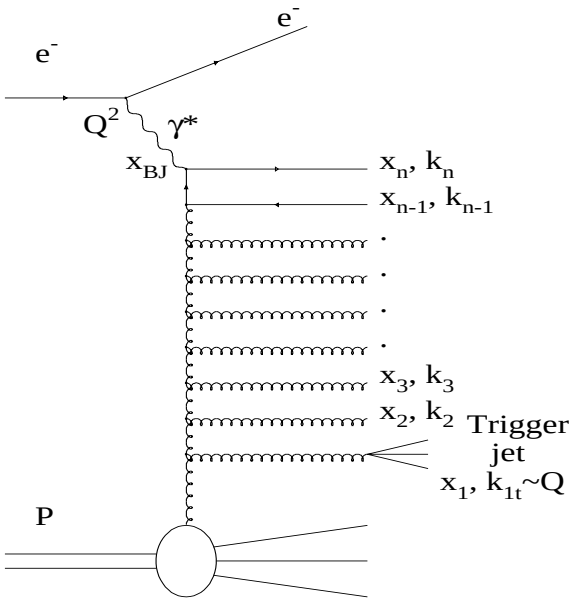

Figure 7: Selection of forward jets in DIS events.

4.3 DIS events with a large rapidity gap

It was anticipated that the HERA collider should provide a rather unique possibility to study diffractive dissociation at short distances [18] and that the rapidity gap would be a powerful criterion to eliminate conventional deep inelastic background. Indeed analysing the 1992 data the ZEUS and H1 collaborations [19, 20] have found that events with a rapidity gap (with respect to the forward LAr limit) $\Delta\eta \geq 2$ amount to about 6 % of the DIS sample. First analyses of data from 1993 confirm this observation and allow us to investigate the origin of those events. Assuming that the proton interacts diffractively, the interaction can be modelled as the exhange of a colourless Regge pole, the pomeron. Two possible mechanisms are considered hereafter.

The first mechanism, based on vector meson dominance of the photon (VMD), is leptoproduction of vector mesons, which can be elastic (Fig.8 a) or followed by soft dissociation of the vector meson (Fig.8 b) or by soft dissociation of the proton (Fig.8 c). Production of vector mesons at high Q^2 has already been observed in fixed target experiments [21, 22].

The second mechanism considers the possibility that any partonic structure of the pomeron, a quark (Fig.8 e) or a gluon (Fig.8 f) is resolved by the high Q^2 photon.

The data used in this analysis correspond to an integrated luminosity of 273 nb^{-1}.

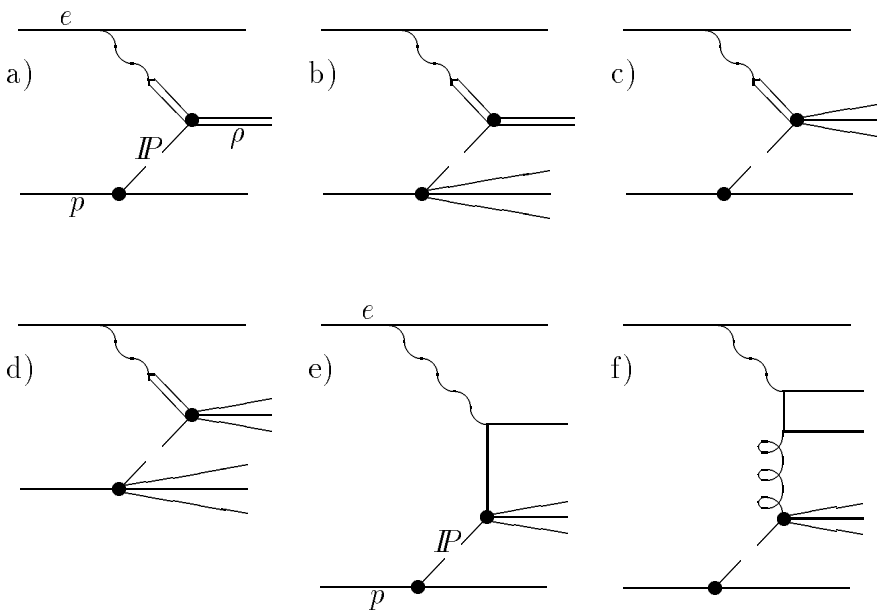

Figure 8: Diagrams which illustrate the VMD and deep inelastic electron pomeron scattering descriptions of the rapidity gap events: a) ρ production via elastic VMD; b) VMD ρ production with soft dissociation of the proton; c) VMD photon interaction followed by soft dissociation of the vector meson; d) VMD photon interaction followed by soft dissociation of both the vector meson and the proton; e) inelastic scattering off a quark in the pomeron; f) inelastic scattering off a gluon in the pomeron via photon gluon fusion.

A total of 14550 DIS events were selected by requiring an electron in the BEMC with an energy of at least 12 GeV and a polar angle θ below 173^0, namely $5 < Q^2 < 100$ GeV^2 and $10^{-4} < x < 10^{-2}$.

A histogram of η_{max}, the largest pseuso-rapidity of each DIS event, Fig.9 a), reveals that in most events there is energy close to $\eta = 3.65$, the largest rapidity which can be measured in the liquid argon calorimeter. There is also a long tail of events with small value of η_{max}. A 5 % fraction of the DIS sample events have a largest rapidity η_{max} below 1.8. The number of events expected in this rapidity gap sample from simulations based on the non diffractive model of deep inelastic scattering LEPTO, which do not include any pomeron exchange, is found to be negligible. The data were also compared with VMD expectations (Fig. 9 a) and with expectations of a model of deep inelastic electron pomeron scattering as implemented in the simulation program RAPGAP [23] (Fig. 9 b). The predictions were normalised to the number of events because the models are not enough constraint to give absolute cross sections.

The shape of the η_{max} distribution can be reproduced by the sum of the VMD and DIS simulations. To fully describe the η_{max} distribution by a sum of conventional DIS and VMD processes, a large fraction of inelastic production is required, but given the uncertainties in the Q^2 dependence both of elastic and of inelastic production in VMD processes, the hypothesis that the rapidity gap data are attributable solely to such processes cannot be rejected.

The shape of the η_{max} distribution can also be reproduced by the sum of the RAPGAP and LEPTO simulations. To discriminate between the two models we have also considered the ratio $R(Q^2)$ of rapidity gap events to all DIS events as a function of Q^2. In x intervals which define regions where the ratio of acceptance of all DIS to diffractive events is not changing with Q^2, the ratio $R(Q^2)$ has no significant dependence on Q^2. This could be interpreted as evidence that the production mechanism for diffractive events is leading twist in QCD [19]. But given the uncertainties in the Q^2 dependence both of elastic and of inelastic production in VMD processes, it is possible to reproduce the flat dependence on Q^2 in a VMD picture by an appropriate choice of the ratio of longitudinal to transverse virtual photon proton total cross sections.

The number of diffractive events in the sample with only two charged tracks of opposite sign is 104, and 32 of these have less than 1 GeV of energy not associated spatially with the charged tracks in the liquid argon calorimeter. The two-track charged particle mass spectrum of these events is shown in Fig.10 assuming both particles are pions. The yield and the shape of the dipion mass spectrum is consistent with the expectations of elastic electroproduction of $\rho(0.770)$, $\omega(0.783)$ and $\phi(1.020)$. The expected number of events, extrapolated from fixed targed experiments, ranges from 25 to 250, pending on the unknown size of the longitudinal contribution.

Summarising this section, it is fair to say that a clear signal of diffractive processes is seen in the DIS sample, but that the interpretation is still debatable. The Q^2 and η_{max} distributions can be reproduced by models based on deep inelastic electron

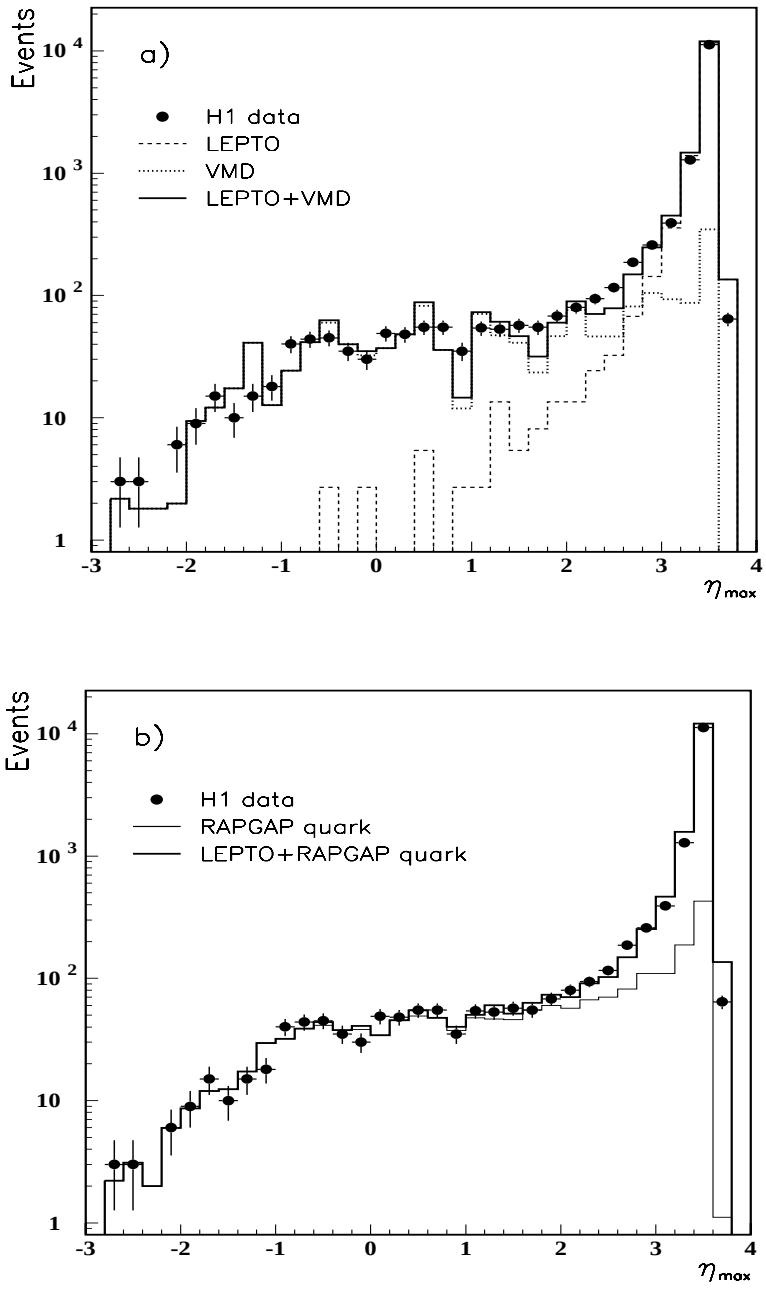

Figure 9: a) Distribution of measured η_{max} for all DIS events with the expectations from LEPTO, from the VMD model and the sum therof. b) Distribution of measured η_{max} for all DIS events with the expectations from LEPTO, from RAPGAP assuming a quark parametrization for the pomeron structure function, and from their sum.

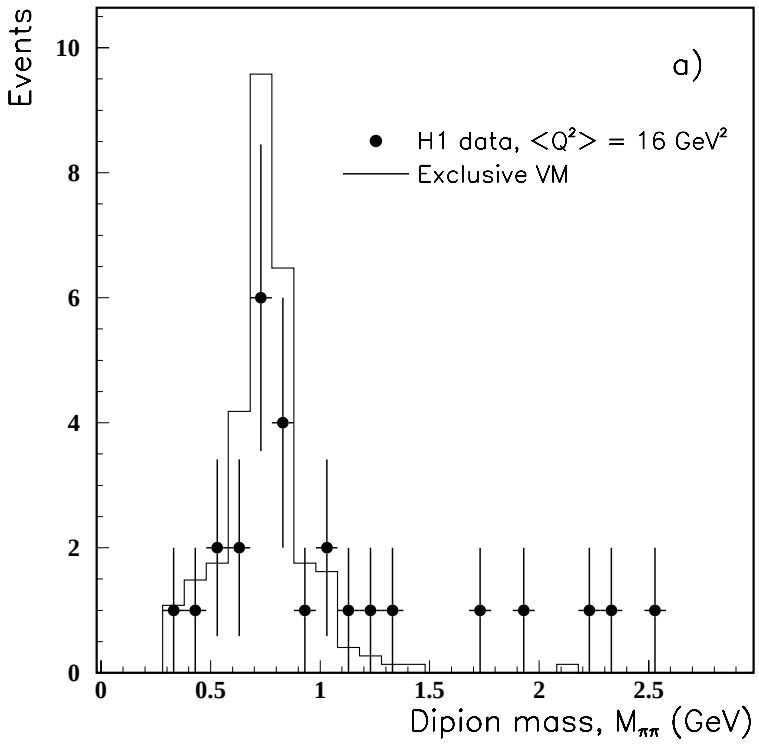

Figure 10: Dipion mass spectrum for oppositely charged two track rapidity gap events with less than $1\,GeV$ additional energy which is not associated with the tracks; the solid line is the expectation from exclusive VMD , including the contributions from ρ production and from kinematic reflections of ω and ϕ production.

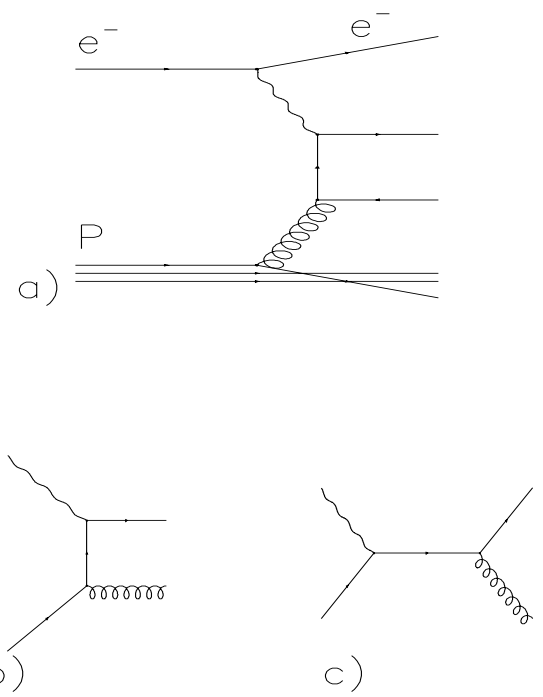

Figure 11: Feynmann diagrams for (2+1) jets in DIS : (a) boson gluon fusion QCD-BGF and (b,c) quark induced QCD-Compton .

pomeron scattering or on VMD contribution. The evidence for elastic vector meson production is not sufficient to estimate the overall contribution of VMD processes.

4.4 α_s measurement from the ratio of (2+1) jet events in DIS

The hadronic final state of deep inelastic events is also a copious source of jets. Radiation of hard gluon from the initial or struck quark, also called QCD-Compton (Fig.11a) or production of a quark anti-quark pair by photon-gluon fusion (Fig11b) together with additional effects of soft gluons and fragmentation are expected to produce several jets in the hadronic final state. Between 10 and 20 % of the DIS events contain (2 + 1) jets (2 high p_t jets and the proton remnant). The production rate is a simple function of $\alpha_s(Q^2)$ and of the gluon density in the proton. With very large statistics it will be possible to fit simultaneously these two quantitities. At present, in one analysis we have used the quark and the gluon densities measured within some errors in fixed target experiments extrapolated to HERA energies and then extracted $\alpha_s(Q^2)$ and in a second analysis we have used the quark densities and the world average of $\alpha_s(Q^2)$ to extract the gluon density in the proton.

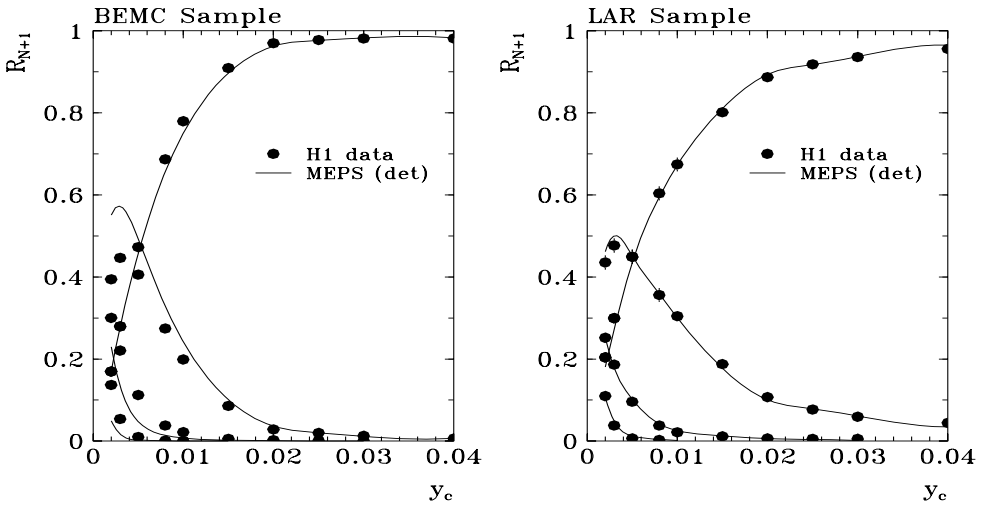

Figure 12: The R_{N+1} distributions from R_{1+1} (top) to R_{4+1} (bottom). The points are the observed jet rates. The full lines represent the Monte Carlo expectations on detector level. The parton density parametrization used is $MRSD^-$.

These studies are based on a sample of DIS events representing an integrated luminosity of about $0.4\,pb^{-1}$. The DIS events are divided into two subsamples with different event selection. The low Q^2 ($Q^2 < 100$ GeV^2) sample consists of events with the scattered electron in the BEMC. The main requirement is a minimum electron energy of 14 GeV, corresponding to $y \leq 0.5$, to eliminate background from photoproduction. The high Q^2 sample consists of events with the scattered electron in the LAr calorimeter with $y \leq 0.7$. After requiring that the squared invariant hadronic mass W^2 is at least 5000 GeV^2, the sample contains 13641 events from the first subsample and 865 events from the second subsample.

Jets are reconstructed from energy clusters in the calorimeters using the JADE algorithm with a pseudoparticle representing the missing longitudinal momentum in the detector. The jet angle in the laboratory system is restricted to $10^0 < \theta_{jet} < 160^0$. The rates R_{N+1} are the ratios of the number of events with N jets inside the calorimeters to the number of events with at least one jet inside the same region. The observed R_{N+1} distributions of the two subsamples are compared on Fig.12 to expectations of the MEPS model. Using this model the corrections to go from the detector level to the parton level are small ($< 15\%$) for $y_c > 0.02$. The MEPS model gives a very good description of the R_{N+1} distribution in the LAr sample for all values of y_c. The low Q^2 sample is described with a similar quality for $y_c > 0.015$. Using this simulation the data are corrected to go from the detector level to the parton level. For a quantitative estimate of the strong running coupling constant we have restricted the evaluation

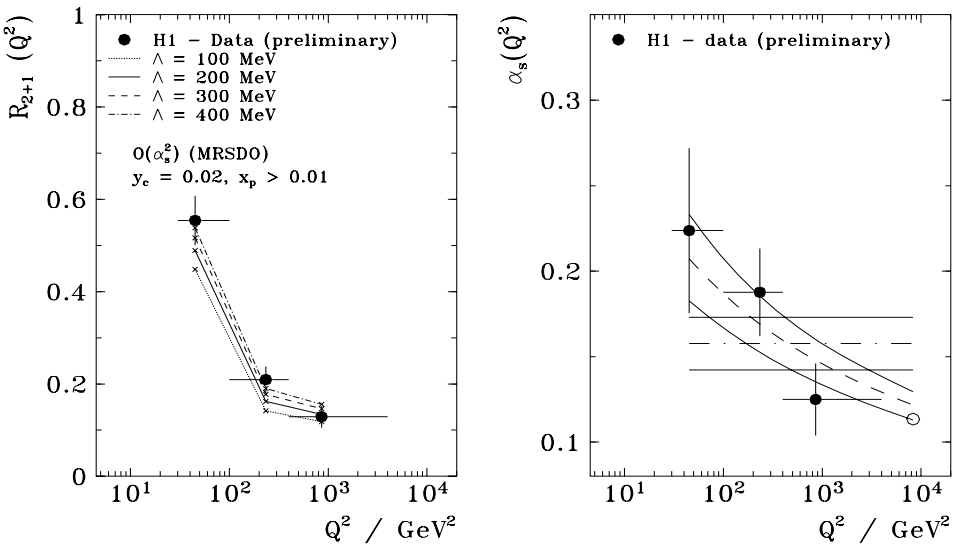

Figure 13: a) The ratio R_{2+1} at $y_c = 0.02$ as a function of Q^2 compared with the PROJET expectations using the $MRSD0$ parametrizations at various Λ values. b)The measured value of α_s as a function of Q^2. The best fit of the running $\alpha_s(Q^2)$ and of the ansatz $\alpha_s = const$ are shown.

to (Q^2, x) regions where the fraction of the proton momentum taken by the struck parton is above 0.01 to reduce the sensistivity to the poorly known parton densities, sea quarks and gluons at very low x. The corrected rates for $y_c = 0.02$ are plotted in Fig.13a) versus Q^2 and compared to the prediction of an analytic calculation PROJET $O(\alpha^2)$ for different values of the usual Λ parameter. The agreement is very good.

The PROJET calculation is used to evaluate the NLO relation between R_{2+1} and α_s in each Q^2 interval for a given set of parton densities. The resulting strong coupling constant is shown in Fig.13 b). The decrease of α_s with Q^2 is seen for the first time from the jet rates in a single experiment. The dashed line represents the best fit of $\alpha_s(Q^2)$ as predicted by the NLO equations of the running coupling constant. Also shown is the ansatz with α_s constant. This ansatz is clearly in conflict with the data. The statistical error is ± 0.009. The preliminary systematic error is ± 0.012 and is dominated by the uncertainties on the parton densities, the energy scale of the calorimeter ($\pm 5\%$) and the scale to be used in the renormalisation group equation that we have varied between $Q^2/4$ and $4Q^2$. The systematic error does not include yet the full uncertainty on the acceptance corrections. The overall preliminary result of $\alpha_s(M_Z^2) = 0.121 \pm 0.015$ is very promising and compares well with $\alpha_s = 0.119 \pm 0.010$ obtained from the LEP experiments with the same observable [25].

4.5 Gluon density from (2+1) jets events in DIS

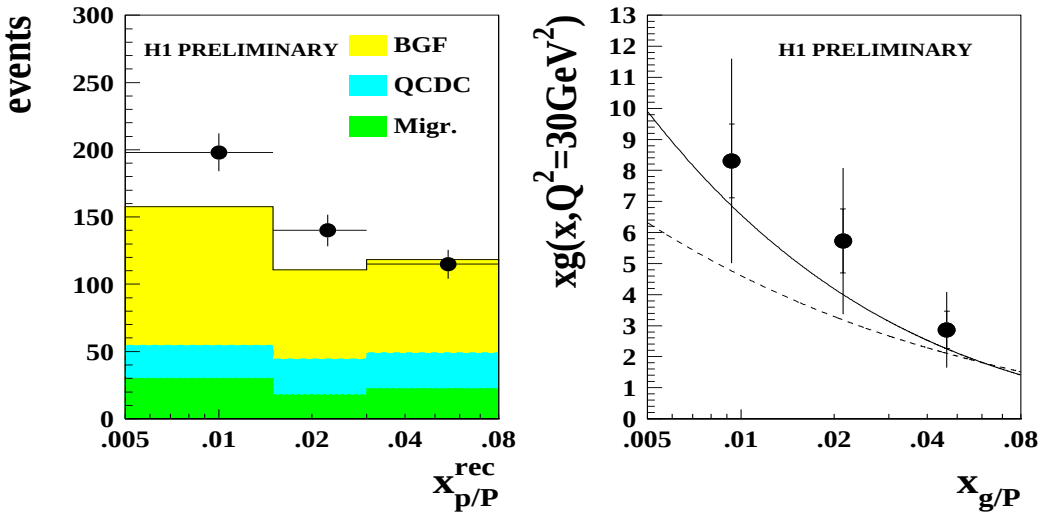

Figure 14: The uncorrected x_p^{rec} distribution (dots) compared to the MEPS expectations (solid). The predictions are broken down into the photon gluon fusion signal for $\hat{s} > 100$ GeV^2, the QCD-Compton background (QCDC) for $\hat{s} > 100$ GeV^2 and the migrations from $\hat{s} < 100$ GeV^2 . b) The LO gluon density $xg(x, Q^2)$ compared to LO GRV (solid) and LO CTEQ2pL (dashed) parametrizations.

In a (2+1) jet event it is possible to reconstruct x_p the fraction of the proton momentum taken by the struck parton :

$$x_p \;=\; x\,(1+\frac{\hat{s}}{Q^2}) \qquad (1)$$

where x is the usual Bjorken scaling variable and $\hat{s}$ is the squared invariant mass of the two-jet system. For events with $\hat{s} > 100$ GeV^2, x_p can be measured with a 30 % resolution. The x_p distribution of the (2+1)jet DIS events with $\hat{s} > 100$ GeV^2 is shown in Fig.14 (a) together with the expectations of a full simulation based on MEPS generators using the MRSH [26] parton densities. In each bin of x_p the expected contributions of photon gluon fusion events and of the background consisting of QCD-Compton events are indicated separately. The amount of low $\hat{s}$ events which migrate into the high $\hat{s}$ acceptance region is also indicated. The model is used to estimate the acceptance corrections to go from the jet level to the parton level and to substract the background events. The corrected x_p distribution of the (2+1) jet events has been compared with expectations of the PROJET analytic calculation using a LO parametrization of the parton densities (GRV[27]) in each bin of x_p to estimate the LO gluon density. The resulting gluon distribution at an average Q^2 value of 30 GeV^2

is shown in Fig.14 (b) and compared with two parametrizations of the LO gluon density ($CTEQ2pL$ [28] and GRV).

The rising of the gluon density with decreasing x is clearly visible. The systematic errors are still large and mainly due to the acceptance corrections.

5. Charged current cross section

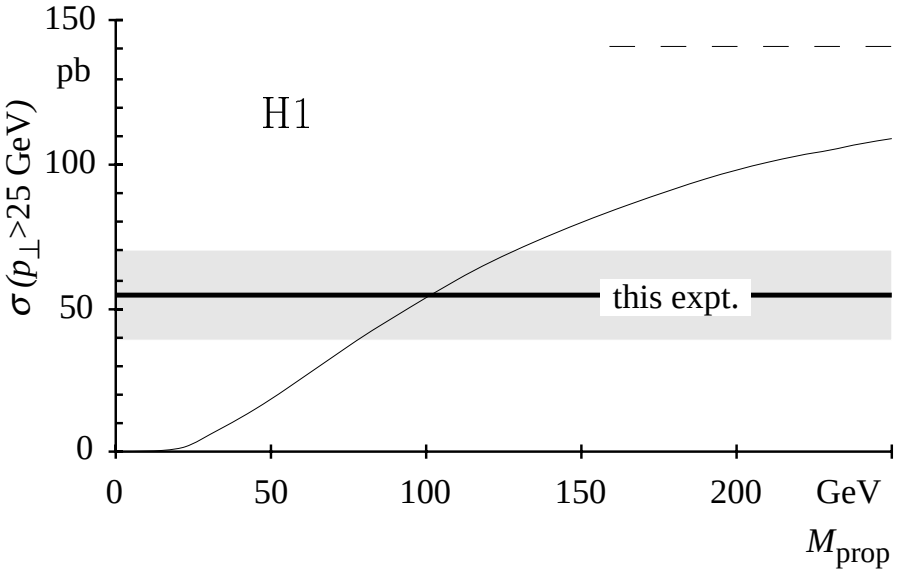

Figure 15: The CC cross section predicted as function of the propagator mass $M_{\rm prop}$ (thin solid line). The dashed line indicates the asymptotic case $M_{\rm prop} = \infty$. The shaded region represents the 1σ band of the measured cross section.

The neutrino-nucleon cross section has been studied for several decades at CERN and FNAL in fixed target experiments. The cross section is proportionnal to the neutrino beam energy, no deviation from linearity has been observed. The ep-collider HERA extends this measurement by exploring, for the first time, the reaction $e^- p \rightarrow \nu_e + hadrons$ in a high energy kinematic region in which the W propagator plays a prominent role. The reaction is the inverse of neutrino-nucleon scattering, where the electron energy corresponds to an equivalent 50 TeV beam energy in a fixed target experiment. The luminosity collected by the H1 experiment during 1993 provides a sufficiently large charged current event sample to exhibit the W propagator effect [29].

The charged current events were selected by requiring a missing transverse energy above 25 GeV. The cut eliminates all background events consisting of DIS neutral

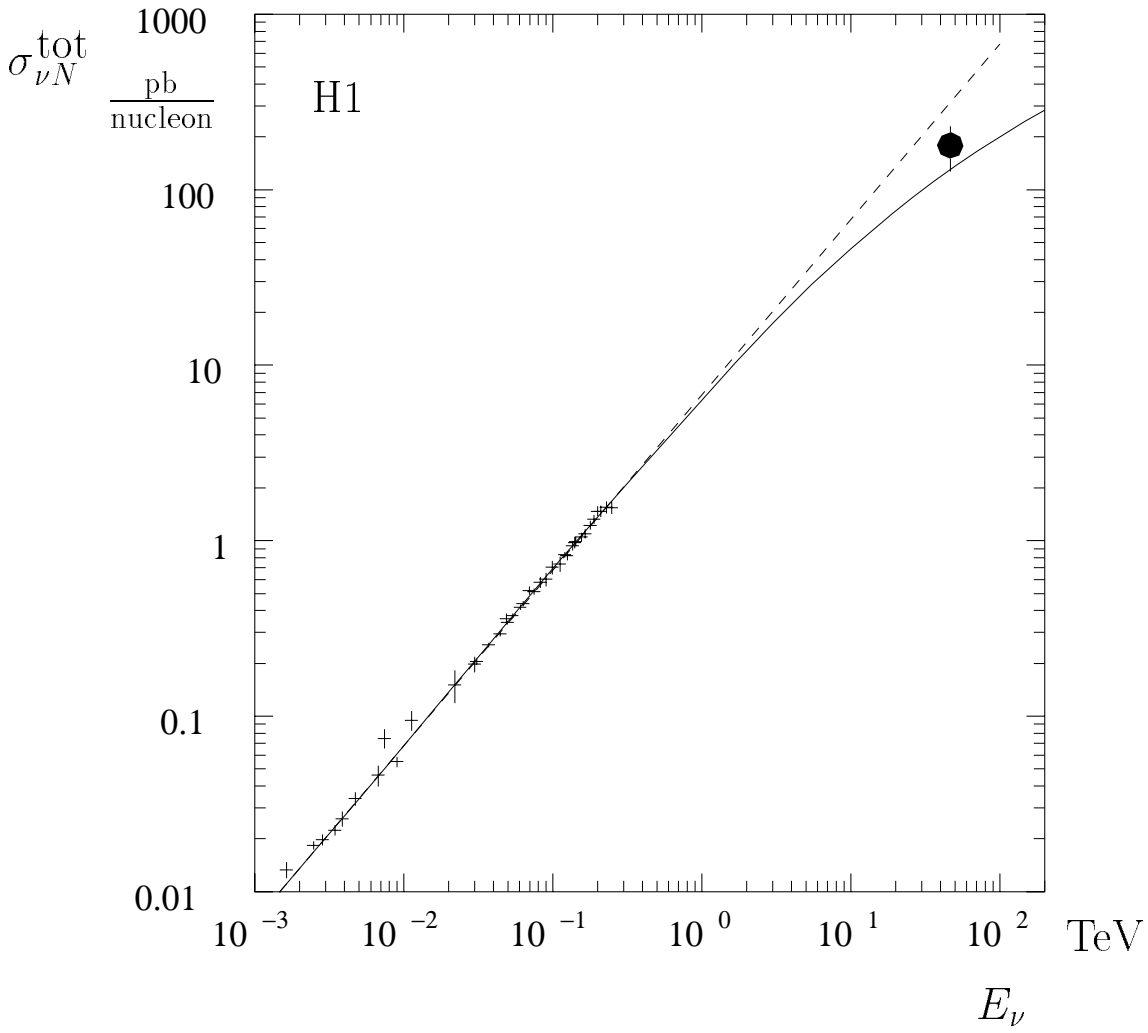

Figure 16: The energy dependence of the νN cross section. The crosses represent the low energy neutrino data (see ref. [30], p. 213) while the full circle refers to the result of this analysis which, for the purpose of comparison, has been converted to a νN cross section. The experiment at HERA corresponds to an equivalent fixed target energy of about 50 TeV. The full line represents the predicted cross section including the W propagator. The dashed line is the linear extrapolation from low energies.

current events as well as all photo-production with a poorly measured hadronic energy. The remaining background is due to cosmic rays or halo muons which are eliminated by appropriate filters. The CC efficiencies have been determined using a NC reference sample obtained by discarding the electron and requiring for the hadron system the same criteria as for CC candidates. The data sample used for the event selection corresponds to an integrated luminosity of $\mathcal{L} = 348 \pm 17\,\mathrm{nb}^{-1}$. After all cuts we are left with a signal of 14 events with an estimated background of 0.1 events. The resulting fully corrected charged current cross section for neutrino transverse momenta $p_\perp > 25\,\mathrm{GeV}$ is

$$\sigma(p_\perp > 25\,\mathrm{GeV}) = 55 \pm 15 \pm 6\,\mathrm{pb},$$

where the first error is statistical and the second one includes all known systematic effects added in quadrature. This experimental value can be compared with the theoretical expectation of 40.9 pb for $p_\perp > 25\,\mathrm{GeV}$.

Fig. 15 shows the sensitivity of the predicted cross section to the propagator mass due to presence of the term $1/(1 + Q^2/M^2_{\mathrm{prop}})^2$. The value of the propagator mass inferred from this measurement agrees well with the known resonance mass of 80.22 GeV [32] and excludes the asymptotic case (dashed line in fig. 15). With the high energy provided by the ep-collider HERA, the effect of the W propagator in deep inelastic charged current interactions is visible for the first time.

For illustration, the measured cross section has been converted into an equivalent νN cross section to be shown in fig. 16. The conversion factor includes the extrapolation of $p_\perp$ to zero based on the parametrization [15, 16] and a reinterpretation as a νN cross section which takes into account the relevant flavour contributions. Note that the extrapolation necessarily reduces the sensitivity to the propagator (cf. fig. 15).

6. Beyond the Standard Model

By exploring a new energy domain at 300 GeV in the $e\,p$ centre of mass HERA has an opportunity to detect signals beyond the Standard Model. There are many processes not yet excluded by the present worldwide data which could be discovered at HERA. The search for new signals can be divided into two groups : either detecting new particles, for example leptoquarks and excited leptons, or indirect detection of new dynamics, through the appearance of small systematic deviations from the expected Standard Model cross sections. Examples of new dynamics are exchange of new bosons W' and Z' or compositeness of leptons and quarks. High luminosity is necessary for detecting small deviations but the hunt for new particles has started from the very first days of $e\,p$ collisions.

At HERA, leptoquarks, with baryon and lepton number conserving couplings, could be produced by fusion of the incident electron and a parton from the proton forming a s-channel resonance. The final state consists of a lepton and a jet coming from the decay of the resonance together with the proton fragments in the beam pipe

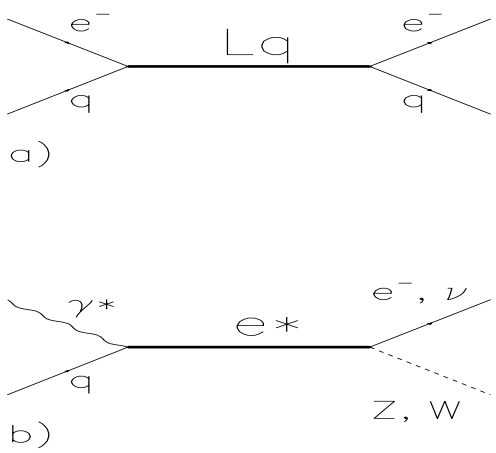

Figure 17: Diagrams describing the formation of new electron-parton (leptoquark, leptogluon, R-parity violating squark) and electron-gauge excited leptons.

and thus cannot be distinguished event per event from a standard DIS event (Fig.17). A leptoquark of mass M would be detected as a narrow peak in the x distribution at $x_0 = M^2/s$ where x_0 is the fractional momentum of the quark which couples to the leptoquark. Neglecting the DIS-LQ interference, the production cross section of a scalar leptoquark would be :

$$\sigma \quad = \quad \frac{\pi}{4M^2}\lambda^2 q(x_0, M) \tag{2}$$

where $q(x_0, Q^2)$ is the quark density in the proton and λ is a dimensionless coupling constant. The usual reference value for λ is 0.31 which corresponds to an electromagnetic coupling, i.e. $\lambda = \sqrt{4\pi\alpha}$. Based on about 400 nb^{-1} no signal has been found in the neutral and charged currents samples (Fig.18). For couplings equal to that of electromagnetic interactions new lower limits at 95% Confidence Level can be assigned, ranging from $M \geq 210$ GeV to $M \geq 250$ GeV for leptoquarks resulting from the fusion of an electron and a quark and from 125 to 170 GeV for leptoquarks formed with an antiquark.

Squarks from R-parity violating supersymmetry could be produced as s -channel resonances between the incoming electron and a parton constituent of the proton. The signature would resemble to that of a leptoquark. To derive limits we have assumed that the squark decays in a photino plus a quark. Rejection limits for different assumptions on the mass the photino are shown on Fig.19.

Leptogluons could also be produced as narrow s-channel resonances at HERA and would look similar to a leptoquark except that the jet would be from a gluon instead

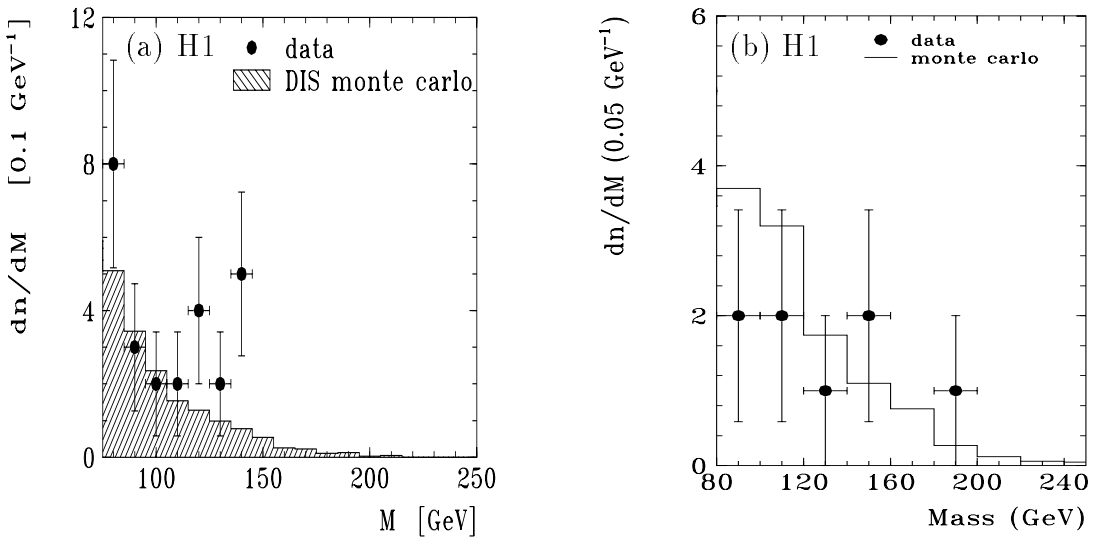

Figure 18: M distribution of (a) NC and (b) CC events. 13 NC events are observed with $M > 100$ GeV (expected are 7.2 events)

of a quark. To lowest order the cross section depends only on the gluon density in the proton and on $(M/\Lambda)^2$, where M is the leptogluon mass and Λ is a scale parameter [34]. H1 excludes the scale region $\Lambda \leq 5$ TeV for $M = 100$ GeV and $\Lambda \leq 1$ GeV for $M = 200$ GeV.

At HERA excited leptons could be produced and the following decays detected (Fig.17): $e^* \rightarrow e\,\gamma, e^* \rightarrow e\,Z, e^* \rightarrow \nu\,W, \nu^* \rightarrow \nu\,\gamma, \nu^* \rightarrow \nu\,Z, or\ \nu^* \rightarrow e\,W$.

In 1992 data, no evidence was found by H1 [33] for the production of e^* or ν^*. So far, only the process $e^* \rightarrow e\,\gamma$ has been studied in the 1993 data. Based on an integrated luminosity of 530 nb^{-1}, we expect 85.5 events with an invariant mass $M_{e\gamma}$ above 10 GeV and have found 85 events (Fig.20 a). Rejection limits with 95 % confidence level are shown in Fig.20 b as a function of the coupling constant $c(\gamma e^* e)$ between the excited electron the electron and the photon.

8. Conclusion

A new set of results of the H1 experiment, based on data recorded in 1993, has provided a new insight into photoproduction, deep inelastic scattering, charged current exchange and produced new limits on searches for new particles. At the time of this workshop, most of the analyses are still preliminary. Many processes are under study. We anticipate within the next months final results on :

-Total cross section in photoproduction

-Bose-Einstein interferometry in photoproduction

-Diffraction and production of elastic vector mesons

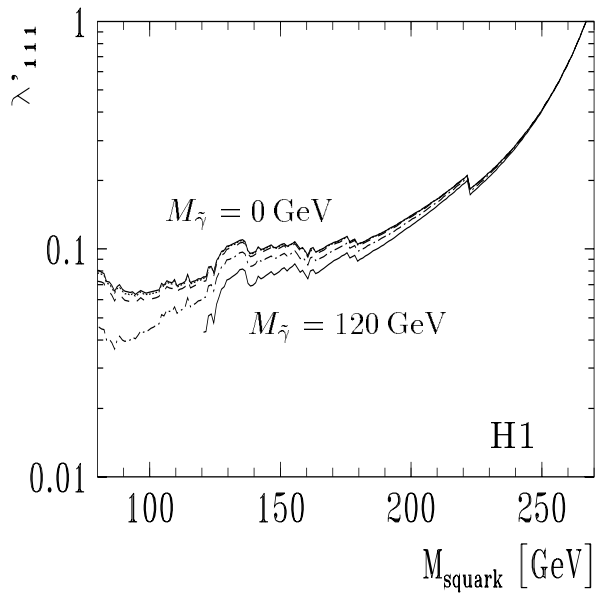

Figure 19: Rejection limits at 95% CL for squarks in a R-parity violating model.

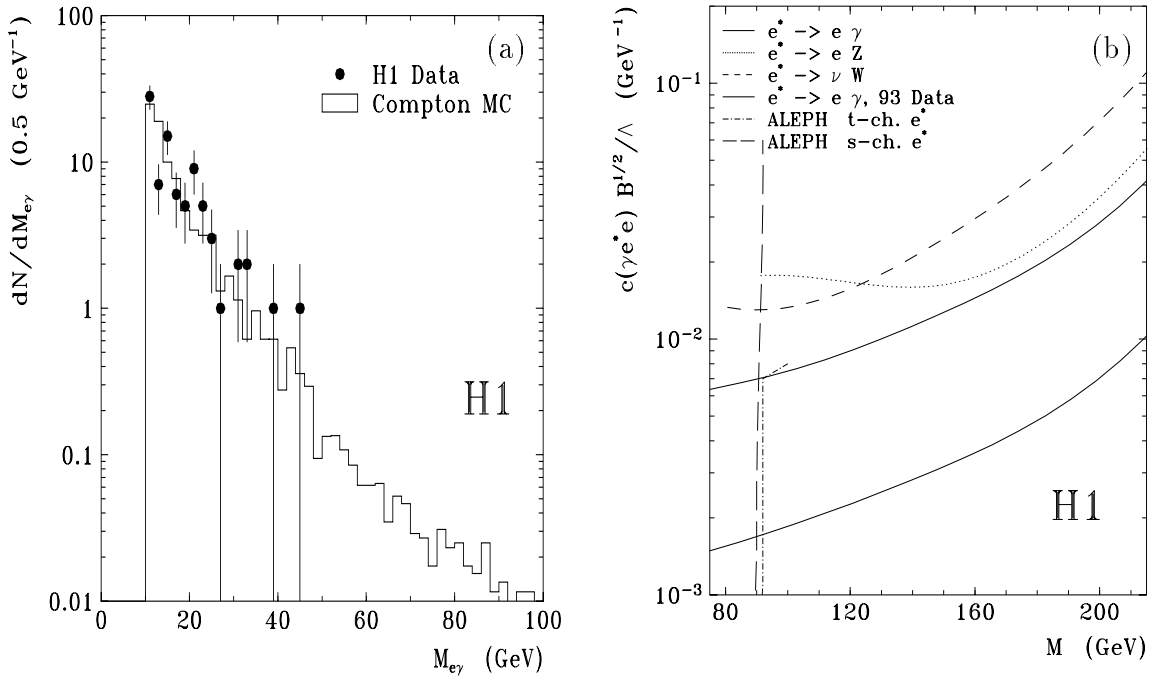

Figure 20: (a) invariant mass of observed $e\gamma$ systems compared with the expected background from Compton processes. (b) Rejection limits at 95% CL for excited electrons decaying in $e\gamma$.

-Production of heavy quarks, J/ψ and D^*
-Hard scattering in photoproduction and measurement of the gluon density in the photon
-The F_2 Structure function of the proton
-Gluon density in the proton from QCD analysis of scaling violation of $F_2(x, Q^2)$
-$\alpha_s(Q^2)$ from the (2+1) jet rate in DIS
-Gluon density in the proton from the (2+1) jet rate in DIS
-Large rapidity gaps in DIS
-Footprints of the BFKL dynamics in DIS

The list is not closed but underlines how rich the physics at HERA is.

References

[1] H1 Collaboration, T. Ahmed et al., DESY 93-103 .

[2] ZEUS Collaboration, The ZEUS Detector, *Technical Proposal* (1986) and The ZEUS Detector, *Status Report 1989.*

[3] R.Eichler,'*Low Q^2 Physics*', this proceeding.

[4] H.-U. Bengtsson and T. Sjöstrand, *Comput. Phys. Commun.***46** (1987) 43 ; T. Sjöstrand, PYTHIA at HERA, *Proc. Workshop on Physics at HERA* (DESY, 1992) 1405.

[5] P.Bruni and G.Ingelman, DESY 93-187, to be published in *Proc. of the Europhysics Conf. on HEP*, Marseille 1993.

[6] E.A.Kuraev, L.N.Lipatov and V.S.Fadin, *Phys.Lett.* **B60** (1975) 50 ; Ya.Ya.Balitski and L.N.Lipatov, *Sov.J.Nucl.Phys.* **28** (1978) 822, *Zh.Eksperiment.I.Teor.Fiz.* **72** (1977) 377.

[7] H1 Collaboration, I. Abt et al., *Nucl. Phys.* **B407** (1993) 515.

[8] ZEUS Collaboration, M. Derrick et al., *Phys. Lett.* **B316** (1993) 412.

[9] M. Bengtsson, G. Ingelman and T. Sjöstrand, *Nucl. Phys.* **B301** (1988) 554.

[10] V.N.Gribov and L.N.Lipatov,*Sov.Journ.Nucl.Phys.* **15** (1972) 438 and 675 G.Altarelli and G.Parisi,*Nucl.Phys.* **126** (1977) 297 Yu.L.Dokshitzer,*Sov.Phys.JETP* **46** (1977) 641.

[11] L. Lönnblad, *Computer Phys. Comm.* **71** (1992) 15.

[12] G.Marchesini et al. *Computer Phys. Comm.* **67** (1992) 465.

[13] H1 Collaboration, I. Abt et al., DESY 94-033, submitted to *Z. Phys. C.*

[14] J.Kwiecinski et al., Durham preprint DTP/94/08 ; see also A.D. Martin, these proceedings.

[15] A.D. Martin, W.J. Strirling, R.G. Roberts, *Phys.Lett.* **B306**, (1993) 145, Erratum **B309** (1993) 492.

[16] A.D. Martin, W.J. Strirling, R.G. Roberts, *Phys.Rev.* **D47** (1993) 867.

[17] A.H. Mueller, *Nucl. Phys. B* (Proc. Suppl.) **18C** (1990) 125 ; J.Phys. G17 (1991) 1443.

[18] M.G.Ryskin and M.Besançon, *Proc. Workshop on Physics at HERA* (DESY, 1992) 215, and references therein.

[19] ZEUS Collaboration, M. Derrick et al. *Phys. Lett.* **B315** 481 (1993).

[20] W. Bartel, "$\sigma_{\gamma p}^{tot}$ and Diffractive Processes in Photoproduction and DIS.", to appear in *Proc. of the Europhysics Conf. on HEP* , Marseille, France, July 1993.
J. B. Dainton, "Results from the H1 Experiment at HERA.", in *Proc. XVI International Symposium on Lepton Photon Interactions*, Cornell, Ithaca, USA, August 1993, Ed. P. Drell and D. Rubin. Rutherford Appleton Laboratory preprint RAL 94-12.
A. De Roeck, "Results from the H1 Experiment.", to appear in *Proc. of the Europhysics Conf. on HEP*, Marseille, France, July 1993. DESY preprint DESY 94-005 (1994).

[21] EMC Collaboration, J. J. Aubert et. al. *Phys. Lett.* **B161** (1985) 203.

[22] NMC Collaboration, P. Amaudruz et. al. *Z. Phys.* **C54** (1992) 239.

[23] H. Jung, "Hard Diffractive Scattering in High Energy *ep* Collisions and the Monte Carlo Generator RAPGAP", DESY preprint DESY 93-182 (1993), submitted to *Comput. Phys. Commun.*

[24] D.Graudenz, PROJET program manual, unpublished.

[25] S.Bethke and J.E. Pilcher, *Annual Review of nuclear and particle science*, **42** (1992) 251.

[26] A.D. Martin and W.J. Stirling "MRS Parton Distribution", RAL Preprint RAL-93-077 (1993)

[27] M. Glück, E. Reya and A. Vogt, *Phys. Rev.* **D46** (1992) 1973
M. Glück, E. Reya and A. Vogt, *Z. Phys.* **C53** (1992) 127.

[28] J.Botts et al., *Phys. Lett.* **B304** (1993) 159.

[29] H1 Collaboration, T. Ahmed et al., *Phys. Lett.* **B323** 241.

[30] D. Haidt and H. Pietschmann: Landolt-Börnstein New Series I/10, Springer (1988)

[31] H. Spiesberger: EPRC91, unpublished program manual, 1991; *Nucl.Phys.* **B349** (1991) 109; *Precision Electroweak Tests at HERA*, preprint Univ. Bielefeld, BI-TP 93/03, Jan. 1993, to be publ. in *Precision Tests of the Standard Model*, Advanced Series on Directions in High Energy Physics, World Scientific Publishing Co., Ed. P. Langacker.

[32] Particle Data Group: *Phys. Rev.* **D45** (1992) II.1 and III.75.

[33] H1 Collaboration, I. Abt et al., *Nucl. Phys.* **B396** (1993) 3.

[34] J.Bijnens, *Proc. Workshop on Physics at HERA* (DESY, 1992) p.819